NeuroImage: Clinical 40 (2023) 103509

Contents lists available at ScienceDirect

NeuroImage: Clinical

journal homepage: www.elsevier.com/locate/ynicl

Quantitative T1 mapping detects blood–brain barrier breakdown in apparently non-enhancing multiple sclerosis lesions

Graziella Donatelli [a,b], Paolo Cecchi [a,b], Gianmichele Migaleddu [a], Matteo Cencini [c], Paolo Frumento [d], Claudio D'Amelio [e], Luca Peretti [b,f], Guido Buonincontri [f], Livia Pasquali [g], Michela Tosetti [f], Mirco Cosottini [e,*], Mauro Costagli [f,h]

[a] Neuroradiology Unit, Azienda Ospedaliero-Universitaria Pisana, Pisa, Italy
[b] Imago7 Research Foundation, Pisa, Italy
[c] National Institute for Nuclear Physics (INFN), Pisa Division, Pisa, Italy
[d] Department of Political Sciences, University of Pisa, Pisa, Italy
[e] Neuroradiology Unit, Department of Translational Research on New Technologies in Medicine and Surgery, University of Pisa, Pisa, Italy
[f] Laboratory of Medical Physics and Magnetic Resonance, IRCCS Stella Maris, Pisa, Italy
[g] Neurology Unit, Department of Clinical and Experimental Medicine, University of Pisa, Pisa, Italy
[h] Department of Neuroscience, Rehabilitation, Ophthalmology, Genetics, Maternal and Child Sciences (DINOGMI), University of Genoa, Genoa, Italy

ARTICLE INFO

Keywords:
Magnetic resonance imaging
Magnetic resonance fingerprinting
Quantitative transient-state imaging
Quantitative imaging
T1 mapping
Multiple sclerosis
Blood-brain barrier

ABSTRACT

Objectives: The disruption of the blood–brain barrier (BBB) is a key and early feature in the pathogenesis of demyelinating multiple sclerosis (MS) lesions and has been neuropathologically demonstrated in both active and chronic plaques. The local overt BBB disruption in acute demyelinating lesions is captured as signal hyperintensity in post-contrast T1-weighted images because of the contrast-related shortening of the T1 relaxation time. On the contrary, the subtle BBB disruption in chronic lesions is not visible at conventional radiological evaluation but it might be of clinical relevance. Indeed, persistent, subtle BBB leakage might be linked to low-grade inflammation and plaque evolution. Here we hypothesised that 3D Quantitative Transient-state Imaging (QTI) was able to reveal and measure T1 shortening (ΔT1) reflecting small amounts of contrast media leakage in apparently non-enhancing lesions (ANELs).

Materials and methods: Thirty-four patients with relapsing remitting MS were included in the study. All patients underwent a 3 T MRI exam of the brain including conventional sequences and QTI acquisitions (1.1 mm isotropic voxel) performed both before and after contrast media administration. For each patient, a ΔT1 map was obtained via voxel-wise subtraction of pre- and post- contrast QTI-derived T1 maps. ΔT1 values measured in ANELs were compared with those recorded in enhancing lesions and in the normal appearing white matter. A reference distribution of ΔT1 in the white matter was obtained from datasets acquired in 10 non-MS patients with unrevealing MR imaging.

Results: Mean ΔT1 in ANELs (57.45 ± 48.27 ms) was significantly lower than in enhancing lesions (297.71 ± 177.52 ms; $p < 0.0001$) and higher than in the normal appearing white matter (36.57 ± 10.53 ms; $p < 0.005$). Fifty-two percent of ANELs exhibited ΔT1 higher than those observed in the white matter of non-MS patients.

Conclusions: QTI-derived quantitative ΔT1 mapping enabled to measure contrast-related T1 shortening in ANELs. ANELs exhibiting ΔT1 values that deviate from the reference distribution in non-MS patients may indicate persistent, subtle, BBB disruption. Access to this information may be proved useful to better characterise pathology and objectively monitor disease activity and response to therapy.

1. Introduction

Multiple sclerosis (MS) is a chronic inflammatory demyelinating, autoimmune and neurodegenerative disease characterised by demyelination, axonal damage, inflammation and gliosis (Reich et al., 2018). The disruption of the blood–brain barrier (BBB) is a key feature in the

* Corresponding author at: Neuroradiology Unit, Azienda Ospedaliero-Universitaria Pisana, Via Paradisa 2, 56124 Pisa, Italy.
E-mail address: mirco.cosottini@unipi.it (M. Cosottini).

https://doi.org/10.1016/j.nicl.2023.103509
Received 21 June 2023; Received in revised form 9 August 2023; Accepted 10 September 2023
Available online 12 September 2023

pathogenesis of MS as it allows inflammatory cells and proteins to enter the nervous tissue and mediate injury to myelin. It has been shown to occur early in the pathogenetic process (Hawkins et al., 1990; Lee et al., 2018; Miller et al., 1988), preceding demyelination and symptom (Kermode et al., 1990; Lee et al., 2018), and has been neuropathologically demonstrated in active but also in chronic lesions (Kermode et al., 1990; Kirk et al., 2003; Kwon and Prineas, 1994; Lee et al., 2018; McQuaid et al., 2009; Vos et al., 2005). The acute inflammation is mediated by activated lymphocytes which penetrate the nervous tissue through an impaired BBB (Minagar and Alexander, 2003), while fibrinogen leaked out of vessels can play a role in chronic inflammation (Lee et al., 2018) as it is able to trigger microglial responses, participate in axonal damage (Davalos et al., 2012) and prevent remyelination (Petersen et al., 2017). In particular, fibrinogen is deposited at the edge of chronic active lesions, where inflammation and active demyelination are also present (Lee et al., 2018), suggesting that those focal lesions may have subtle BBB disruption associated with active demyelination. The ability of proteins and cells to cross an impaired BBB likely depends on a number of factors, such as the extent of vessel injury, cellular size and molecular size of proteins (Hawkins et al., 1990; Kirk et al., 2003). Therefore, different degrees of BBB disruption may have different pathological and clinical implications and different radiological counterparts (Absinta et al., 2016).

In clinical settings, the local overt disruption of the BBB, which is associated with active inflammation (Hawkins et al., 1990; Katz et al., 1993), is captured with T1-weighted magnetic resonance (MR) images acquired after paramagnetic contrast media administration (Grossman et al., 1986). Gadolinium chelated contrast agents shorten the longitudinal (T1) relaxation time of neighbouring water protons, thus increasing signal intensity in post-contrast T1-weighted images. Some attempts have been made in the past to increase the number of visible enhancing lesions (ELs) and improve the detection of contrast enhancement in apparently non-enhancing lesions (ANELs), that are demyelinating MS plaques without visible enhancement in post-contrast conventional imaging. That has been done using triple dose of contrast media to increase the magnitude of enhancement, an off-resonance magnetisation transfer pre-saturation pulse to reduce the signal from the surrounding nervous tissue, and a prolonged delay in post-contrast MR acquisitions to allow more time for the contrast media to cross an impaired BBB (Filippi et al., 1996; Silver et al., 1997). However, these techniques have limitations, as the infusion of an increased dose of contrast media is currently discouraged (Wattjes et al., 2021), focal lesions can appear slightly hyperintense also in pre-contrast magnetisation transfer images when powerful pre-saturation pulses are employed (Mehta et al., 1995), and long post-contrast acquisition delay may be uncomfortable for patients and increase costs. Furthermore, they do not allow to quantitatively measure phenomena associated with the degree of BBB disruption. More recently, semiquantitative and quantitative techniques were used to investigate the integrity of BBB in ANELs, showing respectively increased T1-weighted signal intensity (Silver et al., 2001; Soon et al., 2007a) and T1 relaxation time shortening (Choi et al., 2021; Soon et al., 2007b) after intravenous contrast media administration.

Here we hypothesised that the subtle BBB disruption in ANELs, not visible as contrast enhancement at conventional radiological evaluation, is indeed associated with a quantitatively measurable T1 shortening reflecting small amounts of contrast media leakage. However, contrast enhancement is usually not quantified because the procedure is time-consuming. In the last years, methods for quantitative multiparametric mapping with a single time-efficient acquisition have been developed. These methods include Magnetic Resonance Fingerprinting (MRF) (Ma et al., 2013), Magnetic Resonance Spin TomogrAphy in Time-domain (MR-STAT) (Sbrizzi et al., 2018), quantification using an interleaved Look-Locker acquisition sequence with T2 preparation pulse (QALAS) (Kvernby et al., 2014) and Quantitative Transient-state Imaging (QTI) (Gómez et al., 2020), which provide meaningful quantitative maps of the relaxation times T1 and T2 and of proton density (PD) in clinically feasible acquisition times (Buonincontri et al., 2021). By using such quantitative techniques, quantitative maps of T1 shortening (ΔT1) could be obtained via voxel-wise subtraction of two T1 maps acquired respectively before and after intravenous contrast media administration. To explore this hypothesis, we assessed whether quantitative ΔT1 maps obtained from 3D QTI on a 3 T scanner were able to capture subtle BBB disruption in ANELs.

2. Materials and methods

2.1. Patients

Thirty-four adult patients with relapsing remitting multiple sclerosis (RRMS) (Lublin et al., 2014; Thompson et al., 2018) followed in the neurology outpatient clinic of the University Hospital of Pisa underwent a 3 T MRI exam of the brain with contrast media administration for clinical purposes. During the MRI exam, 25 patients received gadoteridol and 9 patients received gadoteric acid at the recommended dose. For each patient we recorded: disease duration, computed as the number of years elapsed from symptoms onset to MRI examination; clinical disability, assessed with the Expanded Disability Status Scale (EDSS) (Kurtzke, 1983); pharmacological history. Demographic and clinical data of patients are reported in Table 1.

In order to obtain a reference distribution of ΔT1 values in the white matter of subjects without demyelinating lesions, we included in the study also 10 patients (referred to in the text as "non-MS patients") who underwent a 3 T MRI exam of the brain with contrast media administration for clinical purposes (seizures/epilepsy, Bell's palsy, aura, hypoacusis, anosmia) and whose brain imaging was considered unrevealing by two independent neuroradiologists. Five of these patients received gadoteridol and five received gadoteric acid.

This study is part of the research project GR-2016-02361693, approved by the local ethical committee. All patients gave their written informed consent to participate.

2.2. MR data acquisition

All the acquisitions were performed with a 3 T MR system (MR750 scanner, GE Healthcare, Chicago, IL) equipped with an 8-channel head coil. The clinical protocol included the acquisition of MR images both before and after contrast media administration. Before contrast media administration, the protocol included a 3D T1-weighted Fast-Spoiled Gradient-echo (FSPGR, TR = 8.2 ms, TE = 3.2 ms, TI = 450 ms, FA = 12°, spatial resolution = 1 × 1 × 1 mm^3, prescribed parallel to the midsagittal plane) and 3D T2-weighted Fluid Attenuated Inversion Recovery (FLAIR, TR = 7000 ms, effective TE = 114.9 ms, TI = 1943 ms, spatial resolution = 1.2 × 1.2 × 1.2 mm^3, prescribed parallel to the

Table 1
Demographic and clinical data of patients at the time of the MRI examination.

	MS patients	Non-MS patients	p-value
Sex (males/females)	14/20	4/6	>0.5
Age (years) †	41 (31–53)	49 (33–60)	>0.1
Disease duration (years) †	9 (3–18)	–	–
EDSS †	1 (1–2.75) ‡	–	–
Therapy (none/first line/second line) §	7/10/17	–	–

MS, multiple sclerosis.
† Data are expressed as median (interquartile range).
‡ Data of one patient are not available.
§ No treatment (7 patients); first-line treatments (10 patients): INFbeta1a (1), INFbeta1b (1), dimethyl fumarate (6), glatiramer acetate (1), teriflunomide (1); second-line treatments (17 patients): fingolimod (11), natalizumab (5), ocrelizumab (1).

midsagittal plane) sequences. Immediately after contrast media administration, a 3D T1-weighted FSPGR image was acquired (TR = 8 ms, TE = min full, FA = 12°, spatial resolution = 0.94 × 0.94 × 1 mm^3, prescribed parallel to the bicommissural line), followed by a 2D T1-weighted Spin Echo sequence (SE, TR = 440 ms, TE = 10 ms, in-plane resolution = 0.69 × 0.86 mm^2, slice thickness = 4 mm, spacing = 0.5 mm, prescribed parallel to the bicommissural line; acquisition started approximately 4 min after contrast media administration). Besides conventional sequences, two QTI acquisitions were performed before and after contrast media administration (the 2nd QTI acquisition started approximately 9 min after contrast media administration). Each QTI acquisition consisted of an inversion-prepared 3D steady-state free precession sequence with TE/TR = 0.5/8.5 ms and an 880-frame-long variable FA train for T1 and T2 encoding, as shown in Supplementary Fig. S1a. Each frame was sampled with a single interleaf of the 3D spiral projection trajectory shown in Supplementary Fig. S1b and followed by an unbalanced gradient along z direction to reduce B0 sensitivity. The whole acquisition schedule was repeated 56 times to increase the k-space coverage of each frame, resulting in a 1.125 mm isotropic resolution with FOV = 225 mm, whole brain coverage and an acquisition time of 7 min. The sequence is for investigational use and was previously described in detail (Gómez et al., 2020; Kurzawski et al., 2020). Image reconstruction consisted of a zero-filled Non-Uniform Fast Fourier Transform followed by ESPiRIT coil combination (Supplementary Figure S2). Quantitative maps of T1, T2 and proton density (PD) were inferred from the reconstructed images using a neural network (Supplementary Figure S3) trained with a pre-computed dictionary of MR signal evolutions (Gómez et al., 2020).

2.3. MR data post-processing

Pre and post-contrast conventional T1-weighted images of MS patients were visually inspected by two experienced neuroradiologists, who recorded the presence and number of ELs in consensus.

MS white matter lesions were identified on the basis of T2-hyperintense signal and segmented on the conventional T2-weighted FLAIR images by one of the two neuroradiologists using a semi-automated segmentation technique based on user-supervised local thresholding (FSLeyes, https://fsl.fmrib.ox.ac.uk/fsl/fslwiki/FSLeyes). Each lesion was labelled as EL or ANEL according to its radiological properties in conventional post-contrast T1-weighted imaging. Confluent lesions were segmented together as a single lesion whereas non-confluent lesions were labelled as separate lesions.

FSL FAST (Zhang et al., 2001) was used on the brain-extracted (Smith, 2002) pre-contrast T1-weighted images to obtain partial volume maps of white matter, grey matter and cerebrospinal fluid.

For each patient, FSL-FLIRT (Jenkinson et al., 2002) was used to rigidly co-register the pre-contrast FLAIR and T1-weighted images (hence the ROIs covering all FLAIR lesions and the white matter partial volume map) as well as the post-contrast QTI dataset to the pre-contrast QTI scan (Fig. 1A-D). Sinc interpolation was used to co-register the pre-contrast and post-contrast T1 maps. Lesion ROIs (Fig. 1E, red colour) were dilated (Fig. 1G, blue colour) and subtracted to the binarized white matter ROI (Fig. 1G, yellow colour). The resulting mask was eroded to obtain a most conservative NAWM ROI excluding voxels with partial volumes involving MS lesions, cortical grey matter and periventricular cerebrospinal fluid (Fig. 1G and 1H, green colour). The ΔT1 map was obtained by voxel-wise subtraction of the QTI-derived T1 maps acquired respectively before (Fig. 1C) and after intravenous contrast media

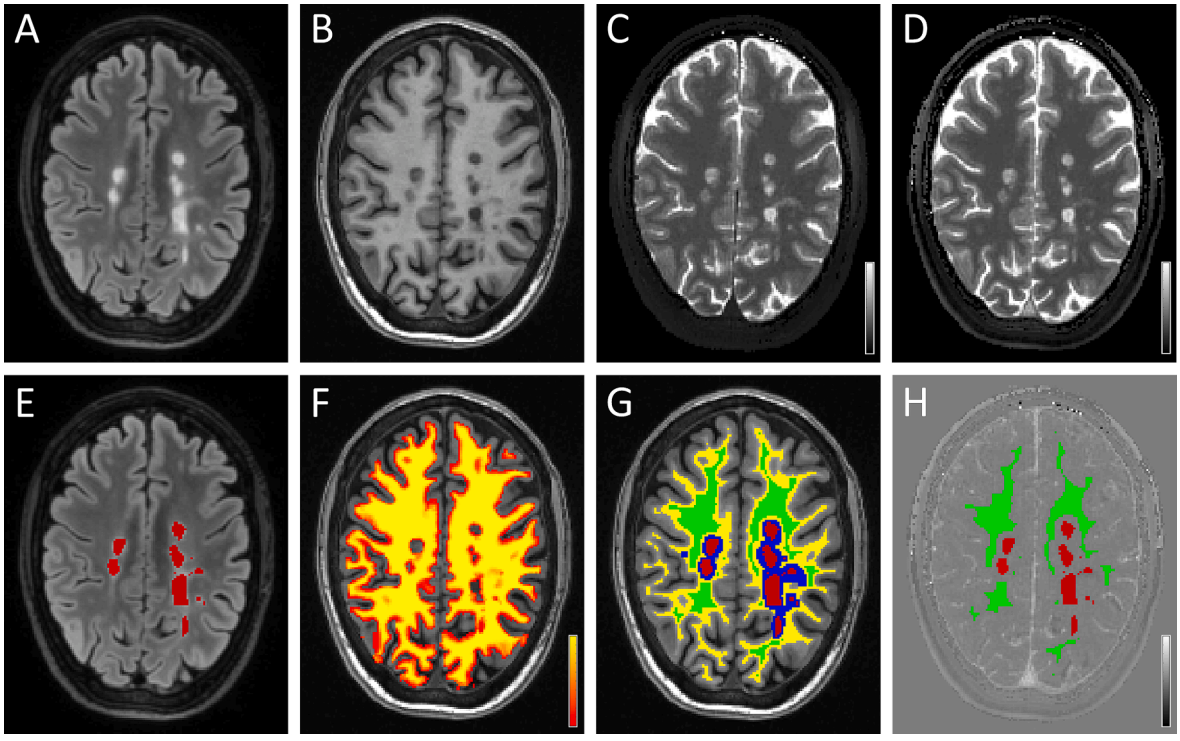

Fig. 1. Representative images obtained in one patient with multiple sclerosis, co-registered to the pre-contrast T1-mapping acquisition. Top row shows pre-contrast FLAIR (A), T1-weighted FSPGR (B) and T1-maps obtained with QTI before (C) and after (D) contrast media administration. Grayscale bars in (C) and (D) cover a range of T1-values between 0 and 3000 ms. In the bottom row: (E) shows lesion ROIs (in red) drawn on the FLAIR image; (F) shows the partial volume map of white matter, ranging between 0 (red) and 100% (yellow), superimposed to the T1-weighted image; (G) shows the ROI representing the normal appearing white matter (NAWM, green), which is defined as the eroded binary mask obtained from the subtraction of dilated lesions (blue) from the binarized white matter map (yellow). ROIs representing multiple sclerosis lesions and NAWM are shown also in (H), superimposed to the quantitative map of contrast-related T1-shortening (ΔT1) after contrast media administration; the bar in (H) ranges between −3000 ms and 3000 ms. (For interpretation of the references to colour in this figure legend, the reader is referred to the web version of this article.)

administration (Fig. 1D).

Then, for each ROI (i.e., ELs, ANELs and NAWM of MS patients, and white matter non-MS patients) number of voxels, ΔT1 mean value and 75th percentile were extracted.

2.4. Data analysis

Differences in sex and age between MS and non-MS patients were tested using respectively the chi-square test and the Mann-Whitney test.

In MS patients, mean ΔT1 values measured in ANELs were compared with those recorded in both ELs and NAWM. The main analysis was conducted by considering all ROIs of size ≥ 27 voxels (0.038 ml) in order to limit the potential detrimental effect of image noise, partial volume occurring during resampling in co-registration and possible imperfect registration; control analyses included also smaller ROIs, of size ≥ 18 and ≥ 12 voxels (corresponding to 0.026 ml and 0.017 ml, respectively). As the BBB disruption might not affect the entire volume of ANELs, also the ROI 75th percentiles of ΔT1 values were considered in the comparisons between ANELs, ELs and NAWM. Data were analysed using linear mixed model to handle repeated measures, with subject identifier as grouping factor.

The association between mean ΔT1 across all ANELs of each patient and EDSS at the time of the MRI examination was investigated using the Spearman's rank correlation test.

Statistical significance for all the analysis was set to 5%.

3. Results

Twenty-one ELs and 2485 ANELs were identified in MS patients on conventional imaging and segmented.

Considering ROIs ≥ 27 voxels, mean ΔT1 in ANELs (mean ± standard deviation = 57.45 ± 48.27 ms) was significantly lower than in ELs (297.71 ± 177.52 ms; $p < 0.0001$) and higher than in NAWM (36.57 ± 10.53 ms; $p < 0.005$) (Fig. 2). Results were confirmed when the same analyses were repeated including also smaller lesions of size ≥ 18 and 12 voxels ($p < 0.0001$ in the comparison between ANELs and ELs, and $p < 0.005$ in the comparison between ANELs and NAWM), and when 75th percentile was analysed ($p < 0.0001$ in all comparisons). Number of ROIs used in each analysis is reported in Table 2.

Sex and age did not significantly differ between MS and non-MS patients (Table 1). Mean ΔT1 of the white matter across non-MS patients had a mean of 37.25 ms and a standard deviation of 8.64 ms. Assuming a normal distribution, these values were used to set to 54.18 ms (ΔT1 mean + 1.96 × standard deviation) the upper limit for the ΔT1 reference range. All ELs and 52% of ANELs exhibited ΔT1 higher than those observed in the white matter of non-MS patients.

Mean ΔT1 across all ANELs of each MS patient was not significantly associated with EDSS at the time of the MRI ($p > 0.05$).

4. Discussion

The aim of this study was to reveal indirect signs of BBB disruption in apparently non-enhancing demyelinating MS lesions with a novel quantitative MRI approach.

QTI-derived quantitative ΔT1 mapping enabled to measure contrast-related T1 shortening in ANELs. ΔT1 in ANELs was significantly higher than in NAWM and lower than in ELs. This result is in line with, and extended, findings of previous studies which estimated T1 values in MS patients using other sequences at different magnetic field strengths, namely serial 2D T1-weighted gradient echo sequences at 1.5 T (Soon et al., 2007b) and a magnetisation-prepared 2 rapid acquisition gradient echoes (MP2RAGE) sequence on a 7 T research scanner (Choi et al., 2021). The lack of a significant association between mean ΔT1 values measured across ANELs and EDSS at the time of MRI examination is not surprising and confirms the result of a previous study (Soon et al., 2007b). Indeed, if subtle BBB leakage in ANELs is associated with chronic low-grade inflammation, the effect of such process on patient disability could be expected to appear later in the follow-up.

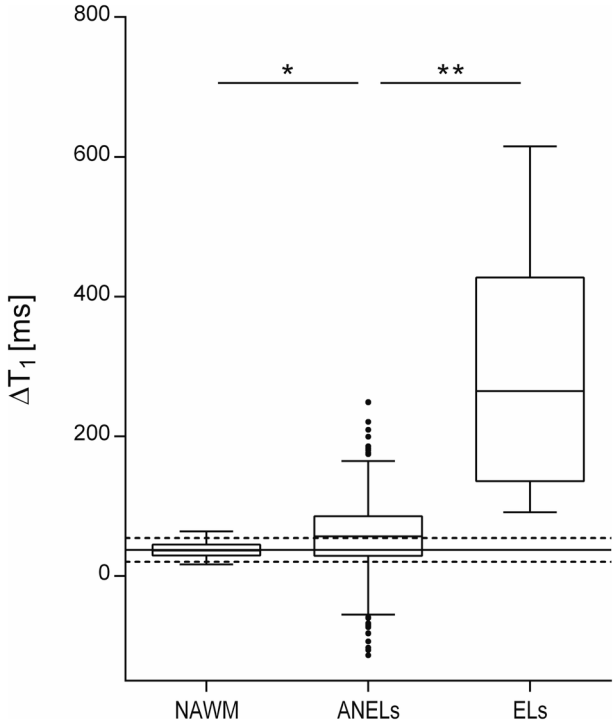

Fig. 2. Boxplot showing differences in ΔT1 between ANELs and NAWM, and between ANELs and ELs. Solid and dashed lines superimposed to the graph represent the reference distribution of white matter ΔT1 values across non-MS patients (mean ± 1.96*standard deviation). NAWM, normal appearing white matter; ANELs, apparently non-enhancing demyelinating multiple sclerosis lesions; ELs, enhancing demyelinating multiple sclerosis lesions. * $p < 0.005$; ** $p < 0.0001$.

Table 2
Number of ROIs and MS patients included in each statistical analysis.

	ROIs ≥ 12 voxels	ROIs ≥ 18 voxels	ROIs ≥ 27 voxels
n. ELs (n. MS patients)	15 (4)	13 (4)	9 (3)
n. ANELs (n. MS patients)	1422 (34)	1105 (34)	844 (34)

ROIs, region of interests; ELs, enhancing demyelinating multiple sclerosis lesions; ANELs, apparently non-enhancing demyelinating multiple sclerosis lesions.

The range of ΔT1 values measured in ANELs extended from low values similar to those in the WM of non-MS patients, up to larger values approaching those measured in ELs. This observation suggests that the presence and degree of BBB disruption vary considerably across this group of lesions. This result could be explained by heterogeneity of lesions belonging to the ANELs group, which likely includes both chronic active and inactive plaques. Pathological studies investigating BBB leakage in chronic lesions were not conclusive, as they agreed on the increased vascular permeability in chronic active lesions but showed conflicting results in chronic inactive lesions (Lee et al., 2018; Vos et al., 2005). The BBB leakage documented in chronic active lesions (together with the ability of fibrinogen to trigger microglial responses, participate in axonal damage (Davalos et al., 2012) and prevent remyelination (Petersen et al., 2017)) fosters future investigation on the possible association between ΔT1 in ANELs and disability accrual. The presence of fibrinogen also in some chronic inactive lesions (Vos et al., 2005) may be related to the diminished fibrinolytic activity in multiple sclerosis (Gveric et al., 2003) or, alternatively, may suggest that the BBB

disruption is not sufficient by itself to induce demyelination (Kwon and Prineas, 1994). Therefore, even though the exact role of BBB impairment in chronic MS lesions is not yet fully understood, it may be linked to the evolution of longstanding demyelinating plaques. Such a subtle BBB disruption cannot be easily and unequivocally assessed using conventional post-contrast T1-weighted images; on the contrary, T1 mapping represents a unique opportunity to objectively detect and measure the effect of contrast media extravasation.

Differently from conventional T1-mapping approaches based on signal fitting of repeated acquisitions, quantitative multiparametric mapping with QTI enables whole brain coverage with high and isotropic resolution in clinically feasible times (Buonincontri et al., 2021; Gómez et al., 2020), is motion robust (Kurzawski et al., 2020) and allows for repeatable and reproducible quantitative T1 mapping (Buonincontri et al., 2021). Taken together, these features make our protocol based on QTI a viable approach to detect subtle BBB leakage. The possibility to objectively detect in vivo the presence, degree and changes over time of subtle BBB disruption may provide new insights into the development and evolution of demyelinating white matter lesions, further evidence for the role of blood-mediated mechanisms in the evolution of chronic lesions, a radiological marker of disease activity and prognosis, and an additional measure of radiological outcome in screening new potential disease-modifying treatments. Furthermore, whether ΔT1 in ANELs or its change over time is proved to be associated with long-term disability, it could be tested as an additional marker of treatment effectiveness and suboptimal response.

Long-term disability prediction in MS is performed with composite outcome measures that combine clinical data and MRI markers of disease activity (Rotstein and Montalban, 2019), but a simple and robust radiological marker of prognosis is still missing (Louapre et al., 2017). Besides the occurrence of new lesions and changes in grey and white matter volume (De Stefano et al., 2014; Inglese and Petracca, 2018; Louapre et al., 2017), chronic inflammation may contribute to disability and disease progression (Absinta et al., 2019) and may account for the substantial functional deterioration which may occur in the absence of new demyelinating lesions (Kermode et al., 1990). The subtle BBB disruption in some ANELs may represent a mechanism reflecting ongoing damage in chronic settings and ΔT1 measurement might have a role as a quantitative biomarker of BBB damage. Future multimodal MR studies investigating ΔT1 in each type of ANELs (e.g., chronic active and chronic inactive lesions) may provide a new piece of knowledge on the inflammatory status of each of them, as revealed by presence and degree of BBB permeability to MRI contrast agent.

To the best of our knowledge, this is the first study investigating the potential of transient-state quantitative multiparametric mapping in capturing pathological enhancement in the brain tissue. This approach allows to obtain quantitative estimations of multiple parameters with only one sequence, thus giving the opportunity to investigate multiple aspects of the MS pathology without the need of multiple acquisitions or image registrations. These advantages, together with the ability to objectively detect subtle BBB disruption, the feasibility of cortical and subcortical segmentation using synthetic T1-weighted images and the possibility to measure relaxometry properties in segmented regions of interest (Fujita et al., 2021), support the use of this technique in the clinical research setting and open the way to a combined qualitative and multiparametric quantitative approach to MS.

This study has some possible limitations. First, most patients were receiving therapy at the time of the MRI examination and drugs administered could have different ability in reducing the vascular permeability or stabilising the BBB (Balasa et al., 2021). Therefore, we cannot exclude that the contrast related T1 shortening we measured was, at least in some patients, influenced by pharmacological treatments. Second, two different paramagnetic contrast media were used across this study; since their difference in T1 relaxivity in human blood samples at 3 T is not statistically significant (Szomolanyi et al., 2019), we do not expect that this limitation could have an impact on our results. Unfortunately, even though the number of ANELs analysed was high, the relatively small number of patients who participated in this study did not allow for subgroup analysis. Future studies investigating the possible role of current and previous therapies as well as the possible impact of different contrast media are advisable. As a third limitation, it cannot be definitely stated that all the ANELs included in the analysis were chronic lesions, because the staging of MS lesions is done at pathological examination of fixed samples. Lastly, we used data acquired in the white matter of non-MS patients to obtain a reference distribution of ΔT1 values. For a more rigorous approach, we would have had to enrol healthy subjects for this purpose, but we preferred not to administer contrast media without a clinical indication.

Each one of the two QTI acquisition, necessary for ΔT1 mapping, has a scan duration of 7 min. Additional scan time could be a possible limitation for the inclusion of this approach in the clinical routine. However, it should be also considered that from the set of quantitative maps obtained from one single QTI acquisition it is possible to generate synthetic radiological images. This approach, known as “synthetic MRI”, aims to obtain diverse contrast-weighted MR images from a small set of tissue parameters (Andica et al., 2019; Blystad et al., 2012; Ji et al., 2022), and is being used in research and clinical MR examinations (Hagiwara et al., 2017; Peretti et al., 2023; Ryu et al., 2020; Tanenbaum et al., 2017). The use of this approach may enable the reduction of the total exam duration, when necessary, by skipping the acquisition of several qualitative images.

In conclusion, QTI-derived quantitative ΔT1 mapping enabled to measure contrast related T1 shortening in ANELs. ANELs exhibiting ΔT1 values that deviate from the reference distribution in non-MS patients may indicate persistent, subtle, BBB disruption. Access to this information may prove useful to better characterise pathology and objectively monitor disease activity and response to therapy.

Funding

This study is part of a research project funded by the Italian Ministry of Health (grant n. GR-2016-02361693). This study was also partially supported by grant RC and the 5 × 1000 voluntary contributions to IRCCS Fondazione Stella Maris, funded by the Italian Ministry of Health.

CRediT authorship contribution statement

Graziella Donatelli: Conceptualization, Methodology, Formal analysis, Investigation, Project administration, Data curation, Visualization, Writing – original draft, Writing – review & editing. **Paolo Cecchi:** Investigation, Data curation, Writing – review & editing. **Gianmichele Migaleddu:** Investigation, Writing – review & editing. **Matteo Cencini:** Software, Visualization, Writing – original draft, Writing – review & editing. **Paolo Frumento:** Supervision, Formal analysis, Writing – review & editing. **Claudio D’Amelio:** Investigation, Writing – review & editing. **Luca Peretti:** Software, Writing – review & editing. **Guido Buonincontri:** Software, Funding acquisition, Writing – review & editing. **Livia Pasquali:** Investigation, Writing – review & editing. **Michela Tosetti:** Resources, Writing – review & editing. **Mirco Cosottini:** Conceptualization, Resources, Supervision, Project administration, Funding acquisition, Writing – review & editing. **Mauro Costagli:** Conceptualization, Methodology, Software, Formal analysis, Investigation, Validation, Data curation, Supervision, Funding acquisition, Project administration, Visualization, Writing – original draft, Writing – review & editing.

Declaration of Competing Interest

The authors declare that they have no known competing financial interests or personal relationships that could have appeared to influence the work reported in this paper.

Data availability

Data will be made available on request.

Appendix A. Supplementary data

Supplementary data to this article can be found online at https://doi.org/10.1016/j.nicl.2023.103509.

References

Absinta, M., Sati, P., Reich, D.S., 2016. Advanced MRI and staging of multiple sclerosis lesions. Nat. Rev. Neurol. 12, 358–368. https://doi.org/10.1038/nrneurol.2016.59.

Absinta, M., Sati, P., Masuzzo, F., Nair, G., Sethi, V., Kolb, H., Ohayon, J., Wu, T., Cortese, I.C.M., Reich, D.S., 2019. Association of Chronic Active Multiple Sclerosis Lesions With Disability In Vivo. JAMA Neurol. 76, 1474–1483. https://doi.org/10.1001/jamaneurol.2019.2399.

Andica, C., Hagiwara, A., Hori, M., Kamagata, K., Koshino, S., Maekawa, T., Suzuki, M., Fujiwara, H., Ikeno, M., Shimizu, T., Suzuki, H., Sugano, H., Arai, H., Aoki, S., 2019. Review of synthetic MRI in pediatric brains: Basic principle of MR quantification, its features, clinical applications, and limitations. J. Neuroradiol. 46, 268–275. https://doi.org/10.1016/j.neurad.2019.02.005.

Balasa, R., Barcutean, L., Mosora, O., Manu, D., 2021. Reviewing the Significance of Blood-Brain Barrier Disruption in Multiple Sclerosis Pathology and Treatment. Int. J. Mol. Sci. 22, 8370. https://doi.org/10.3390/ijms22168370.

Blystad, I., Warntjes, J., Smedby, O., Landtblom, A.-M., Lundberg, P., Larsson, E.-M., 2012. Synthetic Mri of the Brain in a Clinical Setting. Acta Radiol. 53, 1158–1163. https://doi.org/10.1258/ar.2012.120195.

Buonincontri, G., Kurzawski, J.W., Kaggie, J.D., Matys, T., Gallagher, F.A., Cencini, M., Donatelli, G., Cecchi, P., Cosottini, M., Martini, N., Frijia, F., Montanaro, D., Gómez, P.A., Schulte, R.F., Retico, A., Tosetti, M., 2021. Three dimensional MRF obtains highly repeatable and reproducible multi-parametric estimations in the healthy human brain at 1.5T and 3T. Neuroimage 226, 117573. https://doi.org/10.1016/j.neuroimage.2020.117573.

Choi, S., Spini, M., Hua, J., Harrison, D.M., Bergsland, N., 2021. Blood-brain barrier breakdown in non-enhancing multiple sclerosis lesions detected by 7-Tesla MP2RAGE ΔT1 mapping. PLoS One 16 (4), e0249973.

Davalos, D., Kyu Ryu, J., Merlini, M., Baeten, K.M., Le Moan, N., Petersen, M.A., Deerinck, T.J., Smirnoff, D.S., Bedard, C., Hakozaki, H., Gonias Murray, S., Ling, J. B., Lassmann, H., Degen, J.L., Ellisman, M.H., Akassoglou, K., 2012. Fibrinogen-induced perivascular microglial clustering is required for the development of axonal damage in neuroinflammation. Nat. Commun. 3, 1227. https://doi.org/10.1038/ncomms2230.

De Stefano, N., Airas, L., Grigoriadis, N., Mattle, H.P., O'Riordan, J., Oreja-Guevara, C., Sellebjerg, F., Stankoff, B., Walczak, A., Wiendl, H., Kieseier, B.C., 2014. Clinical Relevance of Brain Volume Measures in Multiple Sclerosis. CNS Drugs 28, 147–156. https://doi.org/10.1007/s40263-014-0140-z.

Filippi, M., Yousry, T., Campi, A., Kandziora, C., Colombo, B., Voltz, R., Martinelli, V., Spuler, S., Bressi, S., Scotti, G., Comi, G., 1996. Comparison of triple dose versus standard dose gadolinium-DTPA for detection of MRI enhancing lesions in patients with MS. Neurology 46, 379–384. https://doi.org/10.1212/WNL.46.2.379.

Fujita, S., Buonincontri, G., Cencini, M., Fukunaga, I., Takei, N., Schulte, R.F., Hagiwara, A., Uchida, W., Hori, M., Kamagata, K., Abe, O., Aoki, S., 2021. Repeatability and reproducibility of human brain morphometry using three-dimensional magnetic resonance fingerprinting. Hum. Brain Mapp. 42, 275–285. https://doi.org/10.1002/hbm.25232.

Gómez, P.A., Cencini, M., Golbabaee, M., Schulte, R.F., Pirkl, C., Horvath, I., Fallo, G., Peretti, L., Tosetti, M., Menze, B.H., Buonincontri, G., 2020. Rapid three-dimensional multiparametric MRI with quantitative transient-state imaging. Sci. Rep. 10, 1–17. https://doi.org/10.1038/s41598-020-70789-2.

Grossman, R.I., Gonzalez-Scarano, F., Atlas, S.W., Galetta, S., Silberberg, D.H., 1986. Multiple sclerosis: gadolinium enhancement in MR imaging. Radiology 161, 721–725. https://doi.org/10.1148/radiology.161.3.3786722.

Gveric, D., Herrera, B., Petzold, A., Lawrence, D.A., Cuzner, M.L., 2003. Impaired fibrinolysis in multiple sclerosis: a role for tissue plasminogen activator inhibitors. Brain 126, 1590–1598. https://doi.org/10.1093/brain/awg167.

Hagiwara, A., Hori, M., Yokoyama, K., Takemura, M.Y., Andica, C., Tabata, T., Kamagata, K., Suzuki, M., Kumamaru, K.K., Nakazawa, M., Takano, N., Kawasaki, H., Hamasaki, N., Kunimatsu, A., Aoki, S., 2017. Synthetic MRI in the Detection of Multiple Sclerosis Plaques. Am. J. Neuroradiol. 38, 257–263. https://doi.org/10.3174/ajnr.A5012.

Hawkins, C.P., Munro, P.M.G., Mackenzie, F., Kesselring, J., Tofts, P.S., Boulay, E.P.G.H. DU., Landon, D.N., McDONALD, W.I., 1990. Duration and selectivity of blood-brain barrier breakdown in chronic relapsing experimental allergic encephalomyelitis studied by gadolinium-dtpa and protein markers. Brain 113 (2), 365–378.

Inglese, M., Petracca, M., 2018. MRI in multiple sclerosis: clinical and research update. Curr. Opin. Neurol. 31 (3), 249–255.

Jenkinson, M., Bannister, P., Brady, M., Smith, S., 2002. Improved optimization for the robust and accurate linear registration and motion correction of brain images. Neuroimage 17, 825–841. https://doi.org/10.1016/S1053-8119(02)91132-8.

Ji, S., Yang, D., Lee, J., Choi, S.H., Kim, H., Kang, K.M., 2022. Synthetic MRI: Technologies and Applications in Neuroradiology. J. Magn. Reson. Imaging 55, 1013–1025. https://doi.org/10.1002/jmri.27440.

Katz, D., Taubenberger, J.K., Cannella, B., McFarlin, D.E., Raine, C.S., McFarland, H.F., 1993. Correlation between magnetic resonance imaging findings and lesion development in chronic, active multiple sclerosis. Ann. Neurol. 34, 661–669. https://doi.org/10.1002/ana.410340507.

Kermode, A.G., Thompson, A.J., Tofts, P., Macmanus, D.G., Kendall, B.E., Kingsley, D.P. E., Moseley, I.F., Rudge, P., McDonald, W.I., 1990. Breakdown of the blood-brain barrier precedes symptoms and other MRI signs of new lesions in multiple sclerosis: pathogenetic and clinical implications. Brain 113, 1477–1489. https://doi.org/10.1093/brain/113.5.1477.

Kirk, J., Plumb, J., Mirakhur, M., McQuaid, S., 2003. Tight junctional abnormality in multiple sclerosis white matter affects all calibres of vessel and is associated with blood–brain barrier leakage and active demyelination. J. Pathol. 201, 319–327. https://doi.org/10.1002/path.1434.

Kurtzke, J.F., 1983. Rating neurologic impairment in multiple sclerosis: an expanded disability status scale (EDSS). Neurology 33, 1444–1452. https://doi.org/10.1212/wnl.33.11.1444.

Kurzawski, J.W., Cencini, M., Peretti, L., Gómez, P.A., Schulte, R.F., Donatelli, G., Cosottini, M., Cecchi, P., Costagli, M., Retico, A., Tosetti, M., Buonincontri, G., Costagli, M., Retico, A., Tosetti, M., Buonincontri, G., 2020. Retrospective rigid motion correction of three-dimensional magnetic resonance fingerprinting of the human brain. Magn. Reson. Med. 84, 2606–2615. https://doi.org/10.1002/mrm.28301.

Kvernby, S., Warntjes, M.J.B., Haraldsson, H., Carlhäll, C.-J., Engvall, J., Ebbers, T., 2014. Simultaneous three-dimensional myocardial T1 and T2 mapping in one breath hold with 3D-QALAS. J. Cardiovasc. Magn. Reson. 16, 102. https://doi.org/10.1186/s12968-014-0102-0.

Kwon, E.E., Prineas, J.W., 1994. Blood-brain barrier abnormalities in longstanding multiple sclerosis lesions. An immunohistochemical study. J. Neuropathol. Exp. Neurol. 53, 625–636. https://doi.org/10.1097/00005072-199411000-00010.

Lee, N.J., Ha, S.-K., Sati, P., Absinta, M., Luciano, N.J., Lefeuvre, J.A., Schindler, M.K., Leibovitch, E.C., Ryu, J.K., Petersen, M.A., Silva, A.C., Jacobson, S., Akassoglou, K., Reich, D.S., 2018. Spatiotemporal distribution of fibrinogen in marmoset and human inflammatory demyelination. Brain 141, 1637–1649. https://doi.org/10.1093/brain/awy082.

Louapre, C., Bodini, B., Lubetzki, C., Freeman, L., Stankoff, B., 2017. Imaging markers of multiple sclerosis prognosis. Curr. Opin. Neurol. 30, 231. https://doi.org/10.1097/WCO.0000000000000456.

Lublin, F.D., Reingold, S.C., Cohen, J.A., Cutter, G.R., Sørensen, P.S., Thompson, A.J., Wolinsky, J.S., Balcer, L.J., Banwell, B., Barkhof, F., Bebo, B., Calabresi, P.A., Clanet, M., Comi, G., Fox, R.J., Freedman, M.S., Goodman, A.D., Inglese, M., Kappos, L., Kieseier, B.C., Lincoln, J.A., Lubetzki, C., Miller, A.E., Montalban, X., O'Connor, P.W., Petkau, J., Pozzilli, C., Rudick, R.A., Sormani, M.P., Stüve, O., Waubant, E., Polman, C.H., 2014. Defining the clinical course of multiple sclerosis: The 2013 revisions. Neurology 83, 278–286. https://doi.org/10.1212/WNL.0000000000000560.

Ma, D., Gulani, V., Seiberlich, N., Liu, K., Sunshine, J.L., Duerk, J.L., Griswold, M.A., 2013. Magnetic resonance fingerprinting. Nature 495, 187–192. https://doi.org/10.1038/NATURE11971.

McQuaid, S., Cunnea, P., McMahon, J., Fitzgerald, U., 2009. The effects of blood–brain barrier disruption on glial cell function in multiple sclerosis. Biochem. Soc. Trans. 37, 329–331. https://doi.org/10.1042/BST0370329.

Mehta, R.C., Pike, G.B., Haros, S.P., Enzmann, D.R., 1995. Central nervous system tumor, infection, and infarction: detection with gadolinium-enhanced magnetization transfer MR imaging. Radiology 195, 41–46. https://doi.org/10.1148/radiology.195.1.7892492.

Miller, D.H., Rudge, P., Johnson, G., Kendall, B.E., Macmanus, D.G., Moseley, I.F., Barnes, D., Mcdonald, W.I., 1988. Serial gadolinium enhanced magnetic resonance imaging in multiple sclerosis. Brain 111 (4), 927–939.

Minagar, A., Alexander, J.S., 2003. Blood-brain barrier disruption in multiple sclerosis. Mult. Scler. 9, 540–549. https://doi.org/10.1191/1352458503ms965oa.

Peretti, L.P., Donatelli, G., Cencini, M., Cecchi, P., Buonincontri, G., Cosottini, M., Tosetti, M., Costagli, M., 2023. Generating Synthetic Radiological Images with PySynthMRI: An Open-Source Cross-Platform Tool. Tomography 9 (5), 1723–1733. https://doi.org/10.3390/tomography9050137.

Petersen, M.A., Ryu, J.K., Chang, K.-J., Etxeberria, A., Bardehle, S., Mendiola, A.S., Kamau-Devers, W., Fancy, S.P.J., Thor, A., Bushong, E.A., Baeza-Raja, B., Syme, C. A., Wu, M.D., Coronado, P.E.R., Meyer-Franke, A., Yahn, S., Pous, L., Lee, J.K., Schachtrup, C., Lassmann, H., Huang, E.J., Han, M.H., Absinta, M., Reich, D.S., Ellisman, M.H., Rowitch, D.H., Chan, J.R., Akassoglou, K., 2017. Fibrinogen Activates BMP Signaling in Oligodendrocyte Progenitor Cells and Inhibits Remyelination after Vascular Damage. Neuron 96, 1003–1012.e7. https://doi.org/10.1016/j.neuron.2017.10.008.

Reich, D.S., Lucchinetti, C.F., Calabresi, P.A., 2018. Multiple Sclerosis. N. Engl. J. Med. 378 (2), 169–180.

Rotstein, D., Montalban, X., 2019. Reaching an evidence-based prognosis for personalized treatment of multiple sclerosis. Nat. Rev. Neurol. 15, 287–300. https://doi.org/10.1038/s41582-019-0170-8.

Ryu, K.H., Baek, H.J., Moon, J.I., Choi, B.H., Park, S.E., Ha, J.Y., Jeon, K.N., Bae, K., Choi, D.S., Cho, S.B., Lee, Y., Heo, Y.J., 2020. Initial clinical experience of synthetic MRI as a routine neuroimaging protocol in daily practice: A single-center study. J. Neuroradiol. 47 (2), 151–160.

Sbrizzi, A., van der Heide, O., Cloos, M., van der Toorn, A., Hoogduin, H., Luijten, P.R., van den Berg, C.A.T., 2018. Fast quantitative MRI as a nonlinear tomography problem. Magn. Reson. Imaging 46, 56–63. https://doi.org/10.1016/j.mri.2017.10.015.

Silver, N.C., Good, C.D., Barker, G.J., MacManus, D.G., Thompson, A.J., Moseley, I.F., McDonald, W.I., Miller, D.H., 1997. Sensitivity of contrast enhanced MRI in multiple sclerosis. Effects of gadolinium dose, magnetization transfer contrast and delayed imaging. Brain 120, 1149–1161. https://doi.org/10.1093/brain/120.7.1149.

Silver, N.C., Tofts, P.S., Symms, M.R., Barker, G.J., Thompson, A.J., Miller, D.H., 2001. Quantitative contrast-enhanced magnetic resonance imaging to evaluate blood-brain barrier integrity in multiple sclerosis: a preliminary study. Mult. Scler. 7, 75–82. https://doi.org/10.1177/135245850100700201.

Smith, S.M., 2002. Fast robust automated brain extraction. Hum. Brain Mapp. 17, 143–155. https://doi.org/10.1002/hbm.10062.

Soon, D., Altmann, D.R., Fernando, K.T.M., Giovannoni, G., Barkhof, F., Polman, C.H., O'Connor, P., Gray, B., Panzara, M., Miller, D.H., 2007a. A study of subtle blood brain barrier disruption in a placebo-controlled trial of natalizumab in relapsing remitting multiple sclerosis. J. Neurol. 254, 306–314. https://doi.org/10.1007/s00415-006-0356-z.

Soon, D., Tozer, D., Altmann, D., Tofts, P., Miller, D., 2007b. Quantification of subtle blood-brain barrier disruption in non-enhancing lesions in multiple sclerosis: a study of disease and lesion subtypes. Mult. Scler. 13, 884–894. https://doi.org/10.1177/1352458507076970.

Szomolanyi, P., Rohrer, M., Frenzel, T., Noebauer-Huhmann, I.M., Jost, G., Endrikat, J., Trattnig, S., Pietsch, H., 2019. Comparison of the Relaxivities of Macrocyclic Gadolinium-Based Contrast Agents in Human Plasma at 1.5, 3, and 7 T, and Blood at 3 T. Invest. Radiol. 54 (9), 559–564.

Tanenbaum, L.N., Tsiouris, A.J., Johnson, A.N., Naidich, T.P., DeLano, M.C., Melhem, E. R., Quarterman, P., Parameswaran, S.X., Shankaranarayanan, A., Goyen, M., Field, A.S., 2017. Synthetic MRI for Clinical Neuroimaging: Results of the Magnetic Resonance Image Compilation (MAGiC) Prospective, Multicenter, Multireader Trial. Am. J. Neuroradiol. 38, 1103–1110. https://doi.org/10.3174/ajnr.A5227.

Thompson, A.J., Banwell, B.L., Barkhof, F., Carroll, W.M., Coetzee, T., Comi, G., Correale, J., Fazekas, F., Filippi, M., Freedman, M.S., Fujihara, K., Galetta, S.L., Hartung, H.P., Kappos, L., Lublin, F.D., Marrie, R.A., Miller, A.E., Miller, D.H., Montalban, X., Mowry, E.M., Sorensen, P.S., Tintoré, M., Traboulsee, A.L., Trojano, M., Uitdehaag, B.M.J., Vukusic, S., Waubant, E., Weinshenker, B.G., Reingold, S.C., Cohen, J.A., 2018. Diagnosis of multiple sclerosis: 2017 revisions of the McDonald criteria. The Lancet Neurology 17, 162–173. https://doi.org/10.1016/S1474-4422(17)30470-2.

Vos, C.M.P., Geurts, J.J.G., Montagne, L., van Haastert, E.S., Bö, L., van der Valk, P., Barkhof, F., de Vries, H.E., 2005. Blood–brain barrier alterations in both focal and diffuse abnormalities on postmortem MRI in multiple sclerosis. Neurobiol. Dis. 20, 953–960. https://doi.org/10.1016/j.nbd.2005.06.012.

Wattjes, M.P., Ciccarelli, O., Reich, D.S., Banwell, B., de Stefano, N., Enzinger, C., Fazekas, F., Filippi, M., Frederiksen, J., Gasperini, C., Hacohen, Y., Kappos, L., Li, D. K.B., Mankad, K., Montalban, X., Newsome, S.D., Oh, J., Palace, J., Rocca, M.A., Sastre-Garriga, J., Tintoré, M., Traboulsee, A., Vrenken, H., Yousry, T., Barkhof, F., Rovira, À., Wattjes, M.P., Ciccarelli, O., de Stefano, N., Enzinger, C., Fazekas, F., Filippi, M., Frederiksen, J., Gasperini, C., Hacohen, Y., Kappos, L., Mankad, K., Montalban, X., Palace, J., Rocca, M.A., Sastre-Garriga, J., Tintore, M., Vrenken, H., Yousry, T., Barkhof, F., Rovira, A., Li, D.K.B., Traboulsee, A., Newsome, S.D., Banwell, B., Oh, J., Reich, D.S., Reich, D.S., Oh, J., 2021. 2021 MAGNIMS–CMSC–NAIMS consensus recommendations on the use of MRI in patients with multiple sclerosis. The Lancet Neurology 20, 653–670. https://doi.org/10.1016/S1474-4422(21)00095-8.

Zhang, Y., Brady, M., Smith, S., 2001. Segmentation of brain MR images through a hidden Markov random field model and the expectation-maximization algorithm. IEEE Trans. Med. Imaging 20, 45–57. https://doi.org/10.1109/42.906424.